



Article

Variability in Symbiont Chlorophyll of Hawaiian Corals from Field and Airborne Spectroscopy

Gregory P. Asner^{1,2,*}, Crawford Drury³, Nicholas R. Vaughn¹, Joshua R. Hancock³ and Roberta E. Martin^{1,2}

¹ Center for Global Discovery and Conservation Science, Arizona State University, Hilo, HI 96720, USA; nickvaughn@asu.edu (N.R.V.); roberta.martin@asu.edu (R.E.M.)

² School of Ocean Futures, Arizona State University, Hilo, HI 96720, USA

³ Hawai'i Institute of Marine Biology, University of Hawai'i, Kaneohe, HI 96744, USA; druryc@hawaii.edu (C.D.); hancock9@hawaii.edu (J.R.H.)

* Correspondence: gregasner@asu.edu

Abstract: Corals are habitat-forming organisms on tropical and sub-tropical reefs, often displaying diverse phenotypic behaviors that challenge field-based monitoring and assessment efforts. Symbiont chlorophyll (Chl) is a long-recognized indicator of intra- and inter-specific variation in coral's response to environmental variability and stress, but the quantitative Chl assessment of corals at the reef scale continues to prove challenging. We integrated field, airborne, and laboratory techniques to test and apply the use of reflectance spectroscopy for in situ and reef-scale estimation of Chl *a* and Chl *c2* concentrations in a shallow reef environment of Kāne'ohe Bay, O'ahu. High-fidelity spectral signatures (420–660 nm) derived from field and airborne spectroscopy quantified Chl *a* and Chl *c2* concentrations with demonstrable precision and accuracy. Airborne imaging spectroscopy revealed a 10-fold range of Chl concentrations across the reef ecosystem. We discovered a differential pattern of Chl *a* and Chl *c2* use in symbiont algae in coexisting corals indicative of a physiological response to decreasing light levels with increasing water depth. The depth-dependent ratio of Chl *c2*:*a* indicated the presence of two distinct light-driven habitats spanning just 5 m of water depth range. Our findings provide a pathway for further study of coral pigment responses to environmental conditions using field and high-resolution airborne imaging spectroscopy.

Keywords: coral reef; Hawai'i; hyperspectral; imaging spectroscopy; Symbiodiniaceae



Citation: Asner, G.P.; Drury, C.; Vaughn, N.R.; Hancock, J.R.; Martin, R.E. Variability in Symbiont Chlorophyll of Hawaiian Corals from Field and Airborne Spectroscopy. *Remote Sens.* **2024**, *16*, 732. <https://doi.org/10.3390/rs16050732>

Academic Editors: Laura Martín-García and Manuel Arbelo

Received: 29 January 2024
Revised: 15 February 2024
Accepted: 17 February 2024
Published: 20 February 2024



Copyright: © 2024 by the authors. Licensee MDPI, Basel, Switzerland. This article is an open access article distributed under the terms and conditions of the Creative Commons Attribution (CC BY) license (<https://creativecommons.org/licenses/by/4.0/>).

1. Introduction

Corals are foundational reef-building organisms that are in decline globally due to climate change, pollution, and overfishing [1,2]. These declines have spurred an explosive growth of effort to monitor coral change over time [3]. Spatial extent and bleaching are two commonly reported metrics of coral condition [4,5], but local variability between coral colonies renders field-based methods prone to enormous spatial uncertainties [6], making estimates of coral change difficult to report at the reef level. Beyond spatial extent, a lack of colony-level monitoring over broad areas limits our ability to quantify the range of coral phenotypic responses to external stress [7]. This subsequently impedes our understanding of the coral genotypic diversity needed to predict reef-level changes in coral communities, our ability to strategize for the selection of climate-tolerant corals for propagation and restoration, and our efforts to pursue new conservation approaches based on environmentally relevant traits [8–10].

Whether in situ on reefs or ex situ in laboratory experiments, coral response to stress is readily observed as change in the algal symbiont community, which fixes carbon for coral growth [11,12]. Because the symbionts house the light-capturing apparatus that includes chlorophyll (Chl), changes in coral color are a well-known visual expression of the dynamic, convoluted effect of changing symbiont density and their in vivo pigment concentrations. Field-based monitoring of coral color is usually relegated to qualitative approaches such

as diver-based color cards [13,14]. This works well for determining major changes in symbiont presence, such as during coral bleaching surveys [15]. However, despite efforts to standardize such visual colorimetric methods, there remains a need for increasingly quantitative, physiologically based approaches to support reef research and conservation applications [16]. This is particularly pressing at the ecosystem level, where the full range of coral responses to external stresses occur but are rarely quantified [17].

Remote sensing of coral symbiont pigments has been demonstrated in several study systems [18–20]. From a field-based perspective, spectral measurements of individual coral colonies have yielded demonstrably accurate estimates of Chl concentration [Chl], often in areal units of $\mu\text{g cm}^{-2}$ as employed in this paper. In situ spectral measurements utilize handheld spectrometers in underwater housings, illuminating corals with either ambient or artificial light, to collect reflectance data in the 400–680 nm wavelength range [21]. These data are then used with a subset of harvested corals to calibrate and validate relationships with [Chl], and other pigment concentrations, determined via lab-based wet chemical assays [22,23].

Despite the known accuracy of in situ colony-scale [Chl] estimates using spectrometers, the use of spectral reflectance is more uncertain at the ecosystem level, which requires airborne or satellite-based imaging spectrometers [24]. Moreover, while the determination of live coral and macroalgal cover in shallow reefs has become operational using airborne imaging spectrometers [25–27], the same level of capability has not been achieved in quantifying coral symbiont [Chl]. This is, in part, due to spatial resolution (2 to 60 m) limitations of airborne and space-based sensors. However, it is also due to a limited availability of quantitative research determining relationships between in situ field spectroscopic studies and imaging spectroscopy from aircraft or satellite sensors.

We investigated the relationships linking field-based and airborne spectroscopy to laboratory-derived assays of coral symbiont [Chl], for two common coral genera found in shallow Pacific reefs: *Montipora* and *Porites*. Using Kāneʻohe Bay, Oʻahu, as a model ecosystem, we quantified [Chl] in and among phenotypically diverse coral colonies of 0.5–2 m in diameter [7,8]. This approach provided an opportunity to establish a quantitative relationship between coral symbiont [Chl] and spectral measurements at two scales of measurement: 10 cm in the field and 40 cm from airborne imaging spectroscopy. Findings from this effort build upon previous field-based spectral studies and expand the approach to airborne observational scales as a precursor to further work on more complex reefs in the Pacific region.

2. Materials and Methods

2.1. Field Sites

The study was conducted in the field and from the air at Kāneʻohe Bay on the island of Oʻahu in the State of Hawaiʻi (Figure 1a). Corals of Kāneʻohe Bay exist on a constellation of very shallow patch reefs situated at depths of <1 to 7 m. The two dominant coral species throughout the bay are *Montipora capitata* and *Porites compressa*, comprising more than 90% of the areal extent in the patch reef locations containing live coral cover [7]. Each patch reef is also covered by areas of bare sand and macroalgae.

Across seven patch reefs spanning the environmental gradient of Kāneʻohe Bay [28], a total of 147 coral colonies were selected and tagged in the field (Figure 1a), including 48 colonies of *Montipora* and 99 colonies of *Porites*. For each tagged coral colony, we collected in situ spectral measurements, tissue samples for laboratory-based [Chl] assays, and airborne spectroscopic measurements (Figure 1b,c).

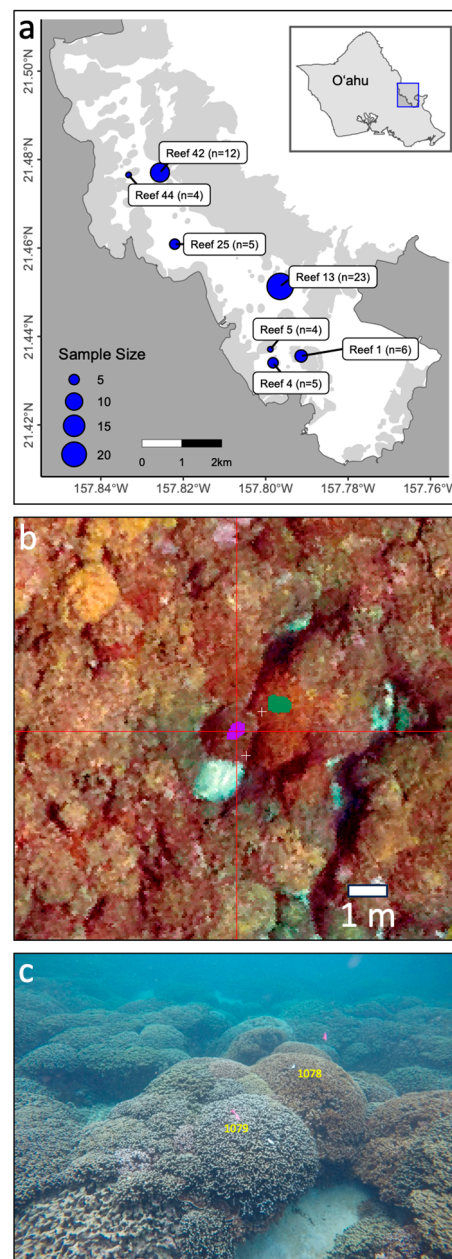


Figure 1. (a) Location and sample distribution of 147 coral colonies throughout Kāneʻohe Bay, Oʻahu, included in the field and airborne spectroscopic study of coral symbiont Chl *a* and Chl *c*2 concentration. (b) Example zoom image and digital tagging of coral colonies selected for field, airborne and laboratory analyses using the Global Airborne Observatory. (c) Underwater photo of the same colonies shown in panel (b).

2.2. Field Measurements

For each tagged coral colony, in situ spectral measurements were collected using an underwater spectrometer (Analytical Spectral Devices HH2-Pro, Boulder, CO, USA) with an underwater halogen light calibrated to the solar spectrum (Keldan Inc., Brugg, Switzerland) operated by two divers. The spectrometer collects spectral radiance measurements in the 400–700 nm range at 1.3 nm full-width at half maximum sampling. We collected three replicate spectra from each coral with the spectrometer fiber cable mounted to the light and placed at a constant distance of 10 cm from the coral colony surface. Immediately prior to each spectral measurement, a reference panel (Spectralon; Labsphere Inc., North Sutton, NH, USA) was used to calibrate each measurement to surface reflectance. The reference

panel was placed within 5 cm of each coral colony in order to control for water depth, water composition, and variable ambient lighting conditions. Reflectance was calculated as the ratio of the measured spectral radiance from the coral colony and the measured spectral radiance from the calibration panel. The derived reflectance spectra were subsequently resampled to 5 nm resolution to match the airborne imaging spectrometer data.

2.3. Laboratory Assays

For each coral colony, we harvested replicate coral branches for subsequent surface area-corrected [Chl] using an acetone extraction from homogenized slurries. Coral branches collected during field surveys were airbrushed using 0.2 μm filtered seawater, and slurry was collected and homogenized for 30 s (Scilogex D-160 Homogenizer, Scilogex Inc., Rocky Hill, CT, USA). A 1 mL aliquot was extracted with acetone following [29], and Chl *a* and Chl *c2* were quantified on a plate reader (SpectraMax M2, Molecular Devices, Sunnyvale, CA, USA) with absorbance read at 650, 663, and 750 nm. Chl *a* is the main pigment in the photosynthetic apparatus of the zooxanthellae, absorbing solar radiation most efficiently in the blue and red parts of the electromagnetic spectrum [30,31]. Chl *c2* is an accessory pigment to Chl *a*, increasing light absorption at a wider range of wavelengths. Concentrations were calculated using the equations of [32] as follows:

$$\begin{aligned}\text{Chl } a &= 11.43 ((A_{663} - A_{750})/\text{PL}) - 0.64 ((A_{630} - A_{750})/\text{PL}) \\ \text{Chl } c2 &= 27.09 ((A_{630} - A_{750})/\text{PL}) - 3.63 ((A_{663} - A_{750})/\text{PL})\end{aligned}$$

where A is absorbance and PL = path length in cm. To standardize to surface area, skeletons were dried for 48 h at 60 °C and weighed. Dried skeletons were dipped for 1 s into paraffin wax at 65 °C, allowed to dry, and re-dipped for 1 s [33]. Surface area standards (1–20 cm²) were used to derive a standard assay curve (R² = 0.99) to calculate the surface area of each fragment [7].

2.4. Airborne Remote Sensing

We collected airborne high-fidelity visible-to-shortwave imaging spectrometer (VSWIR) data with the Global Airborne Observatory (GAO) [34]. The GAO integrates the VSWIR spectrometer with a LiDAR and a 3-channel visible-wavelength 60-megapixel digital camera. During data collection, the aircraft speed was maintained at approximately 105 kts and within 20 m of the nominal planned elevation of 400 m above sea level, yielding a per-pixel resolution of 40 cm. The VSWIR data were collected in 427 wavelength channels between 350 and 2485 nm at 5 nm increments (full-width at half maximum). The high-resolution camera data were collected at 4 cm spatial resolution, boresight-aligned with the VSWIR spectrometer [34]. This facilitated the visual confirmation of each of the tagged coral colonies in the VSWIR data as selected for the study (Figure 1b,c).

Benthic reflectance and water depth retrieval was accomplished using a modified version of the atmospheric removal method [35,36] applied to the GAO VSWIR data [25]. This method uses Bayesian estimation to simultaneously estimate a combination of water properties, water depth, and bottom reflectance. Using the water-leaving reflectance, the benthic reflectance from 400–700 nm and depth were retrieved for each VSWIR pixel. Prior to the application of the derived airborne Partial Least Squares Regression (PLSR) chemometric equations (see Section 2.5) to the GAO imagery, the VSWIR data were pre-processed to classify pixels as live coral, macroalgal, and sand cover fractions using [26,27]. Only pixels classified as live coral cover were subsequently analyzed for Chl *a* and Chl *c2* concentration in units of $\mu\text{g cm}^{-2}$.

2.5. Chemometric Analyses

We used PLSR analysis [37] to develop quantitative chemometric models relating the brightness normalized field and airborne reflectance data to lab-assayed surface area-corrected Chl *a* and Chl *c2* concentrations from coral branches. PLSR is particularly suited for chemometric analyses where the number of input variables is large relative to the

number of observations and collinearity among spectral wavelengths is present [38]. In addition, it is important to utilize the full suite (shape) of spectral data to quantify the convolved signal derived from the chemical constituents, rather than a band-by-band analysis. For the purpose of PLSR model development and testing, data for lab-assayed Chl *a* and Chl *c2* concentrations with their respective spectra, either field or airborne, were randomly split 70:30 percent for ten replicate models. Each model utilizing 70% of the data ($n = 94$ – 111) was constructed using leave-one-out cross-validation. To avoid overfitting, the number of factors used in the PLSR model was determined by minimizing the Prediction Residual Error Sum of Squares (PRESS) statistic [39]. The precision and accuracy of each of the ten model replicates and their test results ($n = 36$ – 53) were assessed based on the coefficient of determination (R^2) and root mean square error (RMSE), respectively, using standard least squares linear regression between the remotely sensed Chl (field or airborne modeled) and lab-assayed Chl values. Final models for Chl *a* and Chl *c2* were generated using all the available data ($n = 147$).

3. Results

3.1. Field and Airborne Spectroscopy

Field spectroscopic measurements revealed a nearly 15-fold range of reflectance values among coral colonies (Figure 2a). *Montipora* colonies had up to 40% lower mean spectral reflectance values (depending upon wavelength) relative to *Porites* colonies. Following brightness normalization to minimize ambient lighting effects [37], the intra-specific spectral variability of the two coral species was greatly reduced but remained distinct from one another (Figure 2b). On average, *Porites* had higher brightness-normalized reflectance in the 420–570 nm range and lower values in the 570–670 nm range compared to *Montipora*.

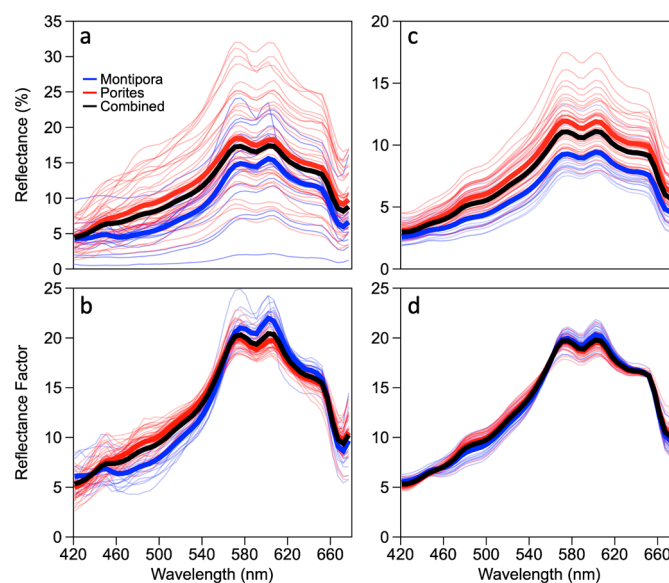


Figure 2. (a) Spectral reflectance and (b) brightness-normalized reflectance of coral colonies collected in situ with an underwater spectrometer. (c) Spectral reflectance and (d) brightness-normalized reflectance of the same coral colonies measured using the Global Airborne Observatory Visible to Shortwave Infrared Imaging Spectrometer (VSWIR). Mean spectra for species shown by thick lines in blue for *Montipora capitata*, red for *Porites compress*, and black for all spectra combined.

A very similar set of patterns was found for the airborne spectroscopic measurements of the collocated coral colonies. We found greater variability and higher reflectance among *Montipora* colonies as compared to *Porites* colonies (Figure 2c). Following brightness normalization, we also found a reduction in intra-specific variability and the same differences in mean reflectance as found with the field-based spectral measurements (Figure 2d).

3.2. Chlorophyll Chemistry

Laboratory-based assays of the coral symbiont [Chl] revealed an extremely wide distribution of Chl *a* (0.47–13.68 $\mu\text{g cm}^{-2}$), and Chl *c2* (0.29–4.43 $\mu\text{g cm}^{-2}$), partially resulting from overall lower concentrations in *Montipora* compared to *Porites* (Figure 3). Overlap of Chl *a* and Chl *c2* among the two coral genera occurred in less than 5% and 10% of field samples, respectively. These chemical differences broadly tracked the observed spectral separability of these coral genera (Figure 2a,c).

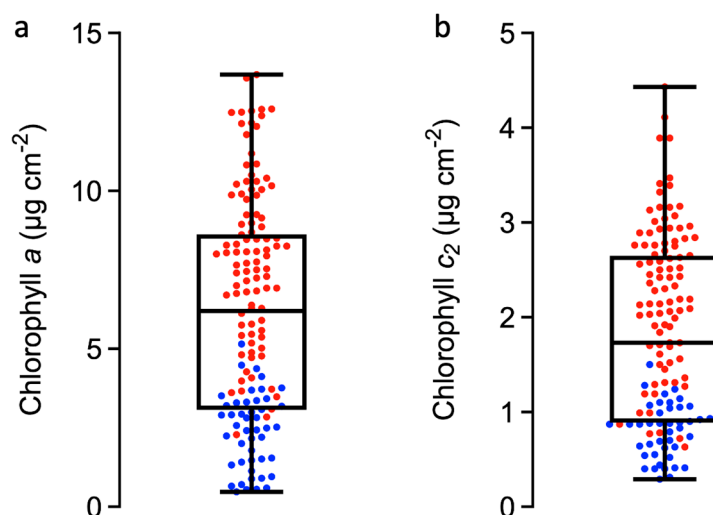


Figure 3. Distribution of (a) Chl *a* and (b) Chl *c2* concentrations derived from laboratory assays of *Porites compressa* (red dots, $n = 99$) and *Montipora capitata* (blue dots, $n = 48$). Box plots indicate means and one standard deviation, and whiskers indicate range.

3.3. Spectroscopic Estimation of Chlorophyll in Corals

Field spectroscopy yielded estimates of Chl *a* and Chl *c2* with demonstrably high precision (R^2) and accuracy (RMSE) (Figure 4a,b, Table 1). The pronounced separation in these spectrally derived concentration estimates between *Montipora* and *Porites* paralleled that of the spectral reflectance (Figure 2) and chemical concentration values (Figure 3). Standardized spectral weightings, derived from the PLSR approach, indicated that the continuous spectrum between 420 nm and 670 nm was required to make the chemical determinations (Figure S1). Whereas some local spectral features emerged with greater importance at around 610 nm, for example, no single reflectance feature proved dominant in the retrieval of Chl *a* or Chl *c2* from the field spectroscopic measurements.

Table 1. Partial least squares regression model results (R^2 ; RMSE; mean standardized % RMSE) for Chl *a* and Chl *c2* derived using field or airborne imaging spectroscopy data. Statistics were generated using ten iterations of randomly selected chlorophyll values from 70% of the data for training ($n = 94$ –111) and 30% for validation ($n = 36$ –53). The resulting number of latent vectors varied between 5 and 15 for models using field spectra and between 8 and 15 for models using airborne spectra. The final model was generated using all the available data ($n = 147$).

		R^2	RMSE	%RMSE
		Chl <i>a</i> ($\mu\text{g cm}^{-2}$)		
Field	Training	0.73 (0.57–0.82)	1.82 (1.50–2.43)	30.08 (25.39–38.38)
	Testing	0.64 (0.54–0.75)	2.17 (1.80–2.75)	34.31 (25.59–41.35)
	Model	0.81	1.53	24.88
Airborne	Training	0.76 (0.57–0.89)	1.67 (1.18–2.39)	27.65 (19.28–38.48)
	Testing	0.61 (0.51–0.73)	2.21 (1.86–2.73)	34.92 (26.01–42.50)
	Model	0.84	1.40	22.76

Table 1. Cont.

		R ²	RMSE	%RMSE
		Chl <i>c</i> 2 ($\mu\text{g cm}^{-2}$)		
Field	Training	0.72 (0.54–0.81)	0.51 (0.42–0.70)	28.69 (22.95–37.63)
	Testing	0.56 (0.37–0.73)	0.65 (0.53–0.82)	35.39 (25.96–44.26)
	Model	0.81	1.53	24.88
Airborne	Training	0.72 (0.47–0.90)	0.51 (0.31–0.76)	28.61 (17.92–40.91)
	Testing	0.53 (0.36–0.71)	0.67 (0.51–0.87)	36.68 (28.22–47.90)
	Model	0.82	0.42	23.20

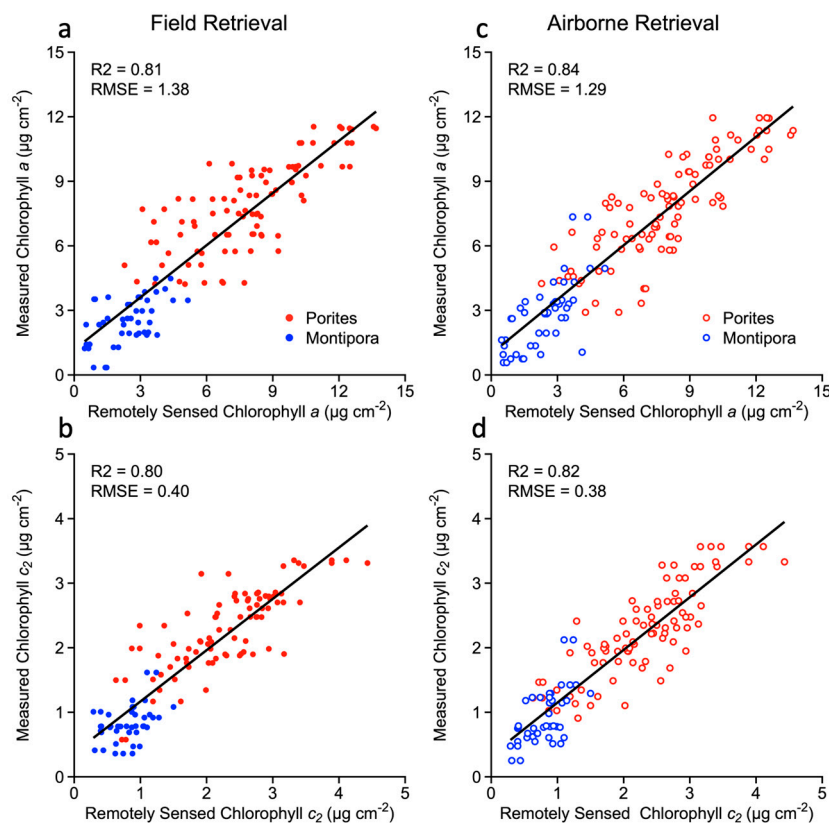


Figure 4. Linear regression between field spectroscopy-based estimates and laboratory-based assays of (a) Chl *a* and (b) Chl *c*2 concentrations. Panels (c,d) are the same but derived from airborne spectroscopy and the same wet chemical assays. *Porites compressa* ($n = 99$) colonies are shown in red and *Montipora capitata* ($n = 48$) colonies are shown in blue.

A similar set of results was derived from the colocated airborne spectroscopic observations (Figure 4c,d). The precision and accuracy of [Chl] estimates rivaled those derived from in situ field spectroscopic estimates (Table 1), and similar to the field-based results, the two coral genera had relatively distinct Chl *a* and Chl *c*2 concentrations, with less than 10% overlap in values (Figure 4c,d).

3.4. Application to Airborne Imaging Spectroscopy

To visualize and assess spatial patterns of Chl *a* and Chl *c*2, we applied the PLSR chemometric calibration equations (from Figures 2d, 3 and S1) to the airborne brightness-normalized bottom reflectance data over the seven patch reefs (Figure 5). Areas of bare sand and macroalgal cover were masked out prior to quantifying coral symbiont Chl concentrations ([Chl], see Section 2). Spatial [Chl] patterns were highly variable by patch reef, with reefs 1, 4, and 5 harboring narrow bands of coral [Chl] that were visually uniform in value (Figure 5a–f). Reefs 13, 25, 42, and 44 were comprised of more coral cover relative to reefs 1, 4, and 5, and they were spatially heterogeneous in both Chl *a* and Chl *c*2

(Figure 5g–r). Reefs 13 and 42 are generally deeper and more variable in depth than the other reefs (>3 m), and thus they contain a wider range of [Chl].

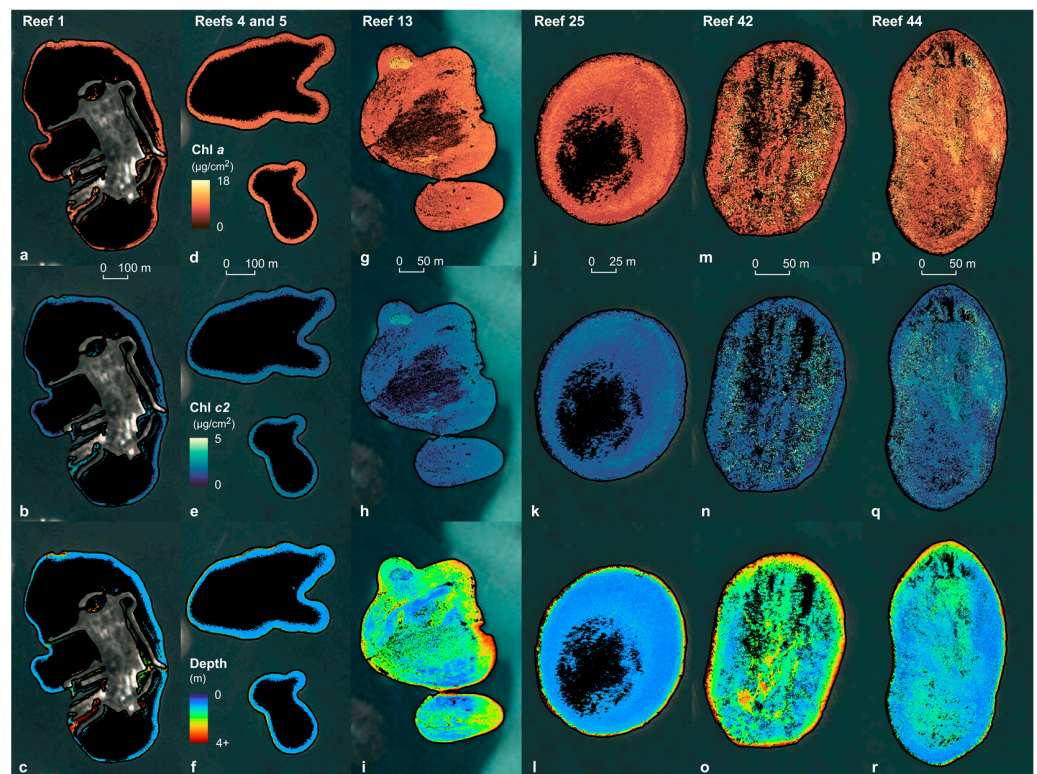


Figure 5. Chl *a* and Chl *c2* concentration estimates in live corals, as well as water depth, derived from airborne imaging spectroscopy collected over Kāneʻohe Bay, Oʻahu, using the Global Airborne Observatory. Black areas are sand and/or macroalgal cover masked prior to coral symbiont Chl estimation. The first, second, and third rows of reefs are for Chl *a*, Chl *c2*, and water depth, respectively. Each column is organized by reef number (1, 4, 5, 13, 25, 42, and 44), as shown in Figure 1. Lettering is organized by reef number: Reef 1 (a–c), Reefs 4–5 (d–f), Reef 13 (g–i), Reef 25 (j–l), Reef 42 (m–o), and Reef 44 (p–r) for Chl *a*, Chl *c2*, and depth, respectively.

Distributions of Chl *a* and Chl *c2* derived from all live coral pixels on each reef further emphasized the pronounced ecological variability of symbiont pigment concentrations (Figure 6). Chl *a* concentrations averaged $9 \mu\text{g cm}^{-2}$, with a slightly skewed distribution to higher values (Figure 6). Chl *c2* averaged $2.3 \mu\text{g cm}^{-2}$ with a slightly negative skew (Figure 6).

We quantified Chl *a* and Chl *c2* relative to water depth (Figure 7). Chl *a* distributions underwent a distinct shift from near normal distribution, with a median value of $8.06 \mu\text{g cm}^{-2}$ in the 0–1 m depth range, to a highly skewed median of $9.14 \mu\text{g cm}^{-2}$ at depths greater than 5 m (Figure 7a, Table 2). In contrast, we found no pattern of Chl *a* variation based on patch reef location (Figure S2, Table 2).

We found a similar overall pattern of increasing Chl *c2* with increasing water depth, but the relative change was even greater for Chl *c2* (49% increase) compared to Chl *a* (13% increase) (Figure 7b, Table 2). These differential rates of increasing pigment concentration with water depth generated a 44% increase in the Chl *c2*:*a* ratio with depth increases from <1 m to >5 m (Figure 7c, Table 2). Finally, on a reef by reef basis, we found no pattern of variation in the distribution of Chl *c2* or ratios of Chl *c2*:*a* (Figure S2, Table 2).

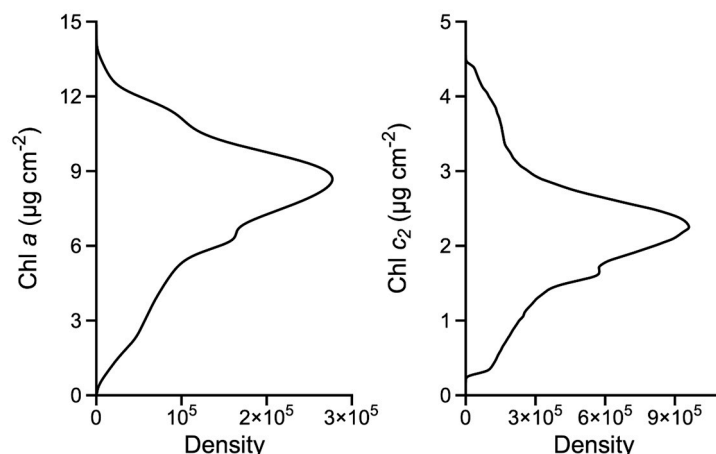


Figure 6. Distributions of coral symbiont Chl *a* and Chl *c2* at 40 cm resolution for all patch reefs combined, derived from airborne imaging spectroscopy.

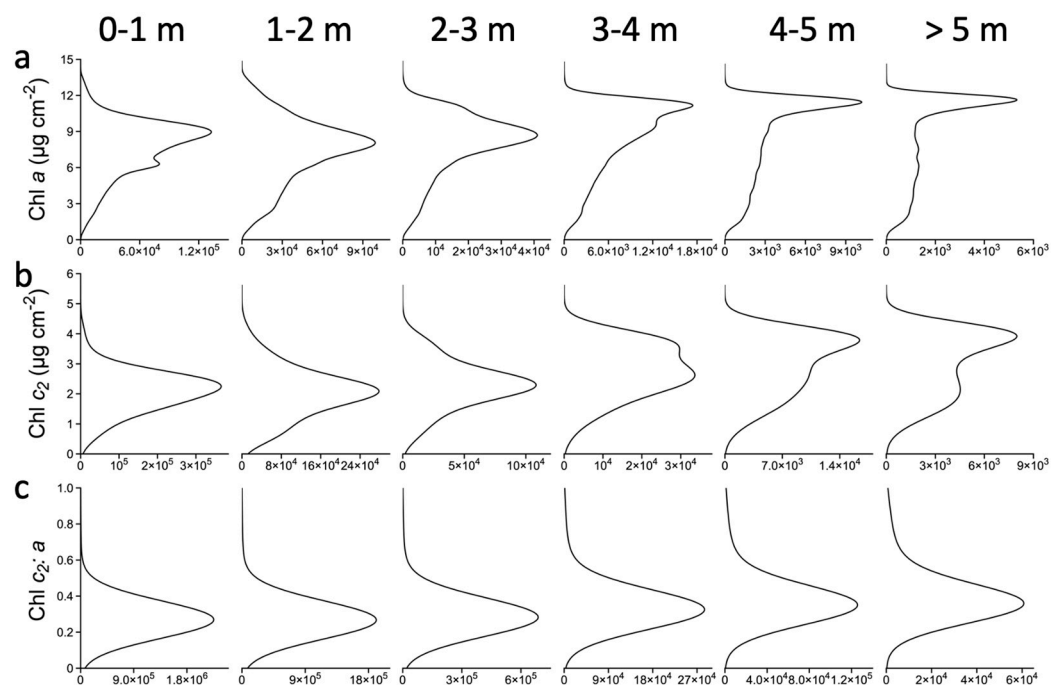


Figure 7. Distributions of (a) Chl *a*, (b) Chl *c2*, and (c) the ratio of Chl *c2*:*a* by water depth for all patch reefs combined, derived from airborne imaging spectroscopy.

Table 2. Total, depth-dependent, and patch reef-dependent statistics for mapped Chl concentrations, and the ratio of chlorophyll *c2*:*a*, including mean, standard deviation (SD), and median.

	No. Samples (Pixels)	Chl <i>a</i> (µg cm ⁻²)		Chl <i>c2</i> (µg cm ⁻²)		Chl <i>c2</i> : <i>a</i>	
		Mean ± SD	Median	Mean ± SD	Median	Mean ± SD	Median
All	1,442,258	7.68 ± 2.49	8.04	2.16 ± 0.78	2.17	0.28 ± 0.06	0.27
			By Depth (m)				
0–1	595,210	7.64 ± 2.26	8.06	2.08 ± 0.65	2.15	0.27 ± 0.05	0.26
1–2	518,693	7.41 ± 2.58	7.73	2.03 ± 0.79	2.05	0.27 ± 0.06	0.26
2–3	190,046	7.97 ± 2.40	8.40	2.30 ± 0.76	2.29	0.29 ± 0.07	0.28
3–4	82,901	8.48 ± 2.73	9.14	2.78 ± 0.85	2.79	0.34 ± 0.09	0.33
4–5	37,112	8.40 ± 3.14	9.30	2.97 ± 0.95	3.13	0.38 ± 0.10	0.35
≥5	18,296	8.27 ± 3.34	9.14	3.00 ± 1.01	3.20	0.39 ± 0.11	0.35

Table 2. Cont.

	No. Samples (Pixels)	Chl <i>a</i> ($\mu\text{g cm}^{-2}$)		Chl <i>c2</i> ($\mu\text{g cm}^{-2}$)		Chl <i>c2:a</i>	
		Mean \pm SD	Median	Mean \pm SD	Median	Mean \pm SD	Median
			By Reef				
Reef 1	326,341	7.87 \pm 2.75	8.30	2.41 \pm 0.91	2.36	0.31 \pm 0.08	0.30
Reef 4 and 5	330,740	8.03 \pm 2.16	8.57	2.23 \pm 0.67	2.29	0.28 \pm 0.06	0.27
Reef 13	394,160	7.55 \pm 2.30	7.98	2.02 \pm 0.66	2.09	0.27 \pm 0.05	0.26
Reef 25	105,985	7.13 \pm 1.78	7.13	1.94 \pm 0.49	1.91	0.28 \pm 0.05	0.26
Reef 42	65,712	6.76 \pm 2.70	7.10	1.99 \pm 0.92	1.97	0.30 \pm 0.08	0.27
Reef 44	219,320	7.62 \pm 2.91	7.69	2.12 \pm 0.90	2.08	0.28 \pm 0.06	0.27

4. Discussion

We integrated field, airborne, and laboratory techniques to test and apply the use of reflectance spectroscopy for in situ and airborne estimations of coral Chl *a* and Chl *c2* concentrations in Hawai'i. The results presented here serve as a step to further operationalize the combined use of field and airborne spectroscopy to map and monitor coral chlorophyll concentration variability in space and time at sub-colony (field) to inter-colony (airborne) resolutions. The applications driving our work range from coral health monitoring, including coral phenotypic bleaching response to environmental stress, to coral restoration planning and outplant performance monitoring. Our findings also build upon and agree with previous work presented at the sub-colony scale [18,19,21,40], which we extend to high-resolution airborne imaging spectroscopy.

Our initial findings indicated that both field and airborne spectroscopy can quantify coral [Chl] in a shallow reef environment, such as Kāne'ohe Bay, with demonstrable precision and accuracy. Often, remote sensing achieves good precision by resolving relative differences in a parameter of interest, but rarely is high accuracy also achieved [24,41,42]. Calibrated bottom reflectance, combined with full-spectrum chemometric techniques, was key to obtaining scale-independent retrievals of [Chl] at the 10 cm field and 40 cm airborne resolutions (Figure 4).

We note that the continuous reflectance spectrum from 420 to 660 nm was critically important to achieving high precision and accuracy results at the field and airborne levels (Figure S1). No one spectral absorption or scattering feature proved more or less important in the spectral analyses, rather the continuum spectral signature carried the signal of differential coral symbiont chlorophyll concentration [22]. This finding is also highly synonymous with similar work on terrestrial plants, suggesting that spectrometers and spectro-chemometric methods, combined with appropriate observational controls, are required [43]. On land, observational controls often include masking out structural gaps in vegetation as well as controlling sun-sensor geometry prior to the chemometric analysis of plant canopies [44]. On reefs, observational controls must focus on the masking of benthic areas without live coral, such as sand and macroalgal patches [45]. Without such controls, the spectral reflectance signature of the benthos is convolved with many features, rendering the retrieval of coral-specific symbiont chemistry an underdetermined spectroscopy problem. For this reason, we masked out sand and macroalgal areas on each patch reef using the method previously presented by Asner et al. [26].

Following the benthic masking process, we used airborne imaging spectroscopy to assess [Chl] variability at the ecosystem scale while maintaining a spatial resolution commensurate with the size of coral colonies found throughout the reef system under study. Doing so revealed new patterns in both Chl *a* and Chl *c2* concentrations at intra- and inter-reef levels (Figure 5). We found a 10-fold range of [Chl] within each patch reef across the bay (Figure S2), suggestive of diverse biotic controls, such as intra- and inter-specific genotypic effects, environmental controls such as light attenuation driven by water depth, and the convolved effects of both types of controls [7].

Despite strong intra-reef variability, the extremely large number of samples derived from airborne spectroscopy revealed systematic increases in Chl *a* and Chl *c2* concentrations

with increasing water depth (Figure 7, Table 2). Both occurred over a relatively narrow depth range of 1 to 5 m, with a pronounced step up in concentration at about 3 m depth. However, we also discovered a differential rate and pattern of Chl *a* and Chl *c2* adjustment with depth. The Chl *c2*:*a* ratio increased markedly with increasing depth, particularly at 3 m and deeper. Chl *a* is the primary light harvesting pigment in the zooxanthae; Chl *c2* is an accessory pigment generated by the symbiont to increase solar energy absorption in lower light environments [31,46,47]. Increasing ratios of Chl *c2*:*a* are thus indicative of decreasing solar irradiance along a gradient of increasing water depth and the physiological response to this limiting resource. We postulate that the 3 m step increase in Chl *c2*:*a* reveals a transition between two distinct physiological regimes in response to light-dependent habitat conditions (sensu [48]). This effect may be due in part to functional diversification of algal symbionts in *Montipora capitata*, which harbors both *Cladocopium* and *Durusdinium* spp. in Kāneʻohe Bay [49]. *Durusdinium*, a highlight specialist symbiont found in shallower depths, strongly influences the metabolic and pigment dynamics in this species [50] and is associated with performance during thermal stress events [51].

Finally, we observed that Chl *c2* variability greatly increased, while Chl *a* variability decreased, with increasing water depth (Figure 7). Decreasing Chl *a* variability is indicative of the physiological limit to adding more Chl *a* as solar irradiance decreases with depth. Spectrally, Chl *a* displays maximum absorption at 440 nm and secondarily at 675 nm [48], and both wavelengths of light are found in abundance in the 0–1 m depth range. At these shallow depths, we observed wide-ranging variability in Chl *a* concentration across all reefs (Figure 7a). Because 675 nm light is strongly attenuated at depths greater than 3 m [52], the distribution of Chl *a* values narrowed with increases in depth, becoming largely dependent on the already highly absorptive 440 nm light that penetrates the water column [23]. This led to a peak investment of about 12 $\mu\text{g cm}^{-2}$ beyond the 4 m depth (Figure 7a). In contrast, Chl *c2* displays peak absorption at 460 nm, but its absorption efficiency is about 50% lower than the 440 nm light absorption in Chl *a* [23]. Nonetheless, light at 460 nm penetrates the water column similarly to 440 nm light [52]. Whereas the investment in Chl *c2* is relatively fixed around 2.3 $\mu\text{g cm}^{-2}$ in the shallowest portion of the reef system, it shifts upward in concentration at depths beyond 3 m (Figure 7b). While we did not attempt to determine the causal mechanisms behind these observed shifts in Chl *a* and *c2*, an enhanced view of chlorophyll variability among corals on reefs provides an avenue to factor physiological patterns into research applications ranging from biogeochemistry to genetics.

A limitation of the current study involves our use of very high spatial resolution (40 cm) airborne imaging spectroscopy, which is not available from satellite sensors. While we did not test the retrievability of coral symbiont chlorophyll concentrations at coarser spatial resolutions, we believe that controlling for inter-colony variability in sand and macroalgal cover does provide some leverage to focus spectroscopy on portions of the reef that are dominated by living corals. This may be translatable to satellite-based observations at coarser resolutions, such as 10–30 m, if similar methods that account for scale-dependent filtering can be applied, such as has been achieved by Zeng et al. [53]. Future research will test this possibility. Additional opportunities may continue to develop for high spatial resolution imaging spectroscopy of reefs, such as with the advent of drone-based imaging spectrometers [54].

Supplementary Materials: The following supporting information can be downloaded at <https://www.mdpi.com/article/10.3390/rs16050732/s1>, Figure S1: Mean and standard deviation of standardized spectral weighting vectors for Partial Least Squares Regression analyses; Figure S2: Distributions of Chl *a*, Chl *c2*, and the ratio of Chl *c2*:*a* by patch reef.; Table S1: In situ chlorophyll concentrations, including mean, standard deviation, and in parentheses, minimum and maximum values for all samples combined as well as by species or each patch.

Author Contributions: Conceptualization, G.P.A., C.D. and R.E.M.; methodology, G.P.A., C.D., N.R.V. and R.E.M.; software, N.R.V.; validation, G.P.A., C.D., J.R.H. and R.E.M.; formal analysis, N.R.V. and R.E.M.; investigation, G.P.A., C.D. and R.E.M.; resources, G.P.A. and C.D.; data curation, N.R.V.;

writing—original draft preparation, G.P.A.; writing—review and editing, G.P.A., C.D., N.R.V. and R.E.M.; funding acquisition, G.P.A. All authors have read and agreed to the published version of the manuscript.

Funding: This research was funded by Paul G Allen Philanthropies grant GPA-2018. The Global Airborne Observatory (GAO) is made possible by support from private foundations, visionary individuals, and Arizona State University.

Data Availability Statement: The data presented in this study are available online at <https://doi.org/10.5281/zenodo.10677026>.

Acknowledgments: We thank C. Balzotti, N. Bean, D. Connetta, S. Decosse, B. Edlund, C. Harris, D. Koopmans, J. Marchiani, and D. Woodward for field, laboratory, and remote-sensing assistance. Coral collections were made under DLNR-DAR permit SAP 2018-03 to the Hawai'i Institute of Marine Biology (HIMB).

Conflicts of Interest: The authors declare no conflicts of interest.

References

1. Veron, J.E.; Hoegh-Guldberg, O.; Lenton, T.M.; Lough, J.M.; Obura, D.O.; Pearce-Kelly, P.; Sheppard, C.R.; Spalding, M.; Stafford-Smith, M.G.; Rogers, A.D. The coral reef crisis: The critical importance of <350 ppm CO₂. *Mar. Pollut. Bull.* **2009**, *58*, 1428–1436. [[CrossRef](#)] [[PubMed](#)]
2. Hughes, T.P.; Barnes, M.L.; Bellwood, D.R.; Cinner, J.E.; Cumming, G.S.; Jackson, J.B.C.; Kleypas, J.; van de Leemput, I.A.; Lough, J.M.; Morrison, T.H.; et al. Coral reefs in the Anthropocene. *Nature* **2017**, *546*, 82–90. [[CrossRef](#)]
3. Obura, D.O.; Aeby, G.; Amorntthamarong, N.; Appeltans, W.; Bax, N.; Bishop, J.; Brainard, R.E.; Chan, S.; Fletcher, P.; Gordon, T.A. Coral reef monitoring, reef assessment technologies, and ecosystem-based management. *Front. Mar. Sci.* **2019**, *6*, 580. [[CrossRef](#)]
4. Eddy, T.D.; Cheung, W.W.L.; Bruno, J.F. Historical baselines of coral cover on tropical reefs as estimated by expert opinion. *PeerJ* **2018**, *6*, e4308. [[CrossRef](#)]
5. Hughes, T.P.; Anderson, K.D.; Connolly, S.R.; Heron, S.F.; Kerry, J.T.; Lough, J.M.; Baird, A.H.; Baum, J.K.; Berumen, M.L.; Bridge, T.C. Spatial and temporal patterns of mass bleaching of corals in the Anthropocene. *Science* **2018**, *359*, 80–83. [[CrossRef](#)]
6. Mumby, P.J.; Skirving, W.; Strong, A.E.; Hardy, J.T.; LeDrew, E.F.; Hochberg, E.J.; Stumpf, R.P.; David, L.T. Remote sensing of coral reefs and their physical environment. *Mar. Pollut. Bull.* **2004**, *48*, 219–228. [[CrossRef](#)] [[PubMed](#)]
7. Drury, C.; Martin, R.E.; Knapp, D.E.; Heckler, J.; Levy, J.; Gates, R.D.; Asner, G.P. Ecosystem-scale mapping of coral species and thermal tolerance. *Front. Ecol. Environ.* **2022**, *20*, 285–291. [[CrossRef](#)]
8. Drury, C.; Lirman, D. Genotype by environment interactions in coral bleaching. *Proc. R. Soc. B* **2021**, *288*, 20210177. [[CrossRef](#)]
9. Lundgren, P.; Vera, J.C.; Peplow, L.; Manel, S.; van Oppen, M.J. Genotype–environment correlations in corals from the Great Barrier Reef. *BMC Genet.* **2013**, *14*, 9. [[CrossRef](#)]
10. Schweinsberg, M.; Weiss, L.C.; Striewski, S.; Tollrian, R.; Lampert, K.P. More than one genotype: How common is intracolony genetic variability in scleractinian corals? *Mol. Ecol.* **2015**, *24*, 2673–2685. [[CrossRef](#)]
11. Baird, A.H.; Bhagooli, R.; Ralph, P.J.; Takahashi, S. Coral bleaching: The role of the host. *Trends Ecol. Evol.* **2009**, *24*, 16–20. [[CrossRef](#)]
12. Knowlton, N. The future of coral reefs. *Proc. Natl. Acad. Sci. USA* **2001**, *98*, 5419–5425. [[CrossRef](#)]
13. Bahr, K.D.; Severino, S.J.; Tsang, A.O.; Han, J.J.; Richards Dona, A.; Stender, Y.O.; Weible, R.M.; Graham, A.; McGowan, A.E.; Rodgers, K.S. The Hawaiian Ko'a Card: Coral health and bleaching assessment color reference card for Hawaiian corals. *SN Appl. Sci.* **2020**, *2*, 1706. [[CrossRef](#)]
14. Siebeck, U.; Marshall, N.; Klüter, A.; Hoegh-Guldberg, O. Monitoring coral bleaching using a colour reference card. *Coral Reefs* **2006**, *25*, 453–460. [[CrossRef](#)]
15. Roth, M.S. The engine of the reef: Photobiology of the coral-algal symbiosis. *Front. Microbiol.* **2014**, *5*, 422. [[CrossRef](#)]
16. Dellisanti, W.; Chung, J.T.; Chow, C.F.; Wu, J.; Wells, M.L.; Chan, L.L. Experimental techniques to assess coral physiology in situ under global and local stressors: Current approaches and novel insights. *Front. Physiol.* **2021**, *12*, 594. [[CrossRef](#)]
17. Donovan, M.K.; Alves, C.; Burns, J.; Drury, C.; Meier, O.W.; Ritson-Williams, R.; Cuning, R.; Dunn, R.P.; Goodbody-Gringley, G.; Henderson, L.M. From polyps to pixels: Understanding coral reef resilience to local and global change across scales. *Landsc. Ecol.* **2023**, *38*, 737–752. [[CrossRef](#)]
18. Hedley, J.D.; Mumby, P.J. Biological and remote sensing perspectives of pigmentation in coral reef organisms. *Adv. Mar. Biol.* **2002**, *43*, 277–317. [[PubMed](#)]
19. Torres-Perez, J.L.; Guild, L.S.; Armstrong, R.A.; Corredor, J.; Zuluaga-Montero, A.; Polanco, R. Relative Pigment Composition and Remote Sensing Reflectance of Caribbean Shallow-Water Corals. *PLoS ONE* **2015**, *10*, e0143709. [[CrossRef](#)] [[PubMed](#)]
20. Hochberg, E.J.; Apprill, A.M.; Atkinson, M.J.; Bidigare, R.R. Bio-optical modeling of photosynthetic pigments in corals. *Coral Reefs* **2006**, *25*, 99–109. [[CrossRef](#)]

21. Joyce, K.E.; Phinn, S.R. Hyperspectral analysis of chlorophyll content and photosynthetic capacity of coral reef substrates. *Limnol. Oceanogr.* **2003**, *48*, 489–496. [[CrossRef](#)]
22. Torres-Pérez, J.; Guild, L.; Armstrong, R. Hyperspectral Distinction of Two Caribbean Shallow-Water Corals Based on Their Pigments and Corresponding Reflectance. *Remote Sens.* **2012**, *4*, 3813–3832. [[CrossRef](#)]
23. Hochberg, E. Spectral reflectance of coral reef bottom-types worldwide and implications for coral reef remote sensing. *Remote Sens. Environ.* **2003**, *85*, 159–173. [[CrossRef](#)]
24. Hedley, J.D.; Roelfsema, C.M.; Chollett, I.; Harborne, A.R.; Heron, S.F.; Weeks, S.; Skirving, W.J.; Strong, A.E.; Eakin, C.M.; Christensen, T.R. Remote sensing of coral reefs for monitoring and management: A review. *Remote Sens.* **2016**, *8*, 118. [[CrossRef](#)]
25. Thompson, D.R.; Hochberg, E.J.; Asner, G.P.; Green, R.O.; Knapp, D.E.; Gao, B.-C.; Garcia, R.; Gierach, M.; Lee, Z.; Maritorena, S. Airborne mapping of benthic reflectance spectra with Bayesian linear mixtures. *Remote Sens. Environ.* **2017**, *200*, 18–30. [[CrossRef](#)]
26. Asner, G.P.; Vaughn, N.R.; Heckler, J.; Knapp, D.E.; Balzotti, C.; Shafron, E.; Martin, R.E.; Neilson, B.J.; Gove, J.M. Large-scale mapping of live corals to guide reef conservation. *Proc. Natl. Acad. Sci. USA* **2020**, *117*, 33711–33718. [[CrossRef](#)]
27. Asner, G.P.; Vaughn, N.R.; Martin, R.E.; Foo, S.A.; Heckler, J.; Neilson, B.J.; Gove, J.M. Mapped coral mortality and refugia in an archipelago-scale marine heat wave. *Proc. Natl. Acad. Sci. USA* **2022**, *119*, e2123331119. [[CrossRef](#)]
28. Caruso, C.; Rocha de Souza, M.; Ruiz-Jones, L.; Conetta, D.; Hancock, J.; Hobbs, C.; Hobbs, C.; Kahkejian, V.; Kitchen, R.; Marin, C. Genetic patterns in *Montipora capitata* across an environmental mosaic in Kāneʻohe Bay, Oʻahu, Hawaiʻi. *Mol. Ecol.* **2022**, *31*, 5201–5213. [[CrossRef](#)]
29. Fitt, W.K.; McFarland, F.K.; Warner, M.E.; Chilcoat, G.C. Seasonal patterns of tissue biomass and densities of symbiotic dinoflagellates in reef corals and relation to coral bleaching. *Limnol. Oceanogr.* **2000**, *45*, 677–685. [[CrossRef](#)]
30. Jiang, J.; Zhang, H.; Kang, Y.; Bina, D.; Lo, C.S.; Blankenship, R.E. Characterization of the peridinin-chlorophyll a-protein complex in the dinoflagellate *Symbiodinium*. *Biochim. Biophys. Acta* **2012**, *1817*, 983–989. [[CrossRef](#)]
31. Niedzwiedzki, D.M.; Jiang, J.; Lo, C.S.; Blankenship, R.E. Spectroscopic properties of the Chlorophyll a-Chlorophyll c 2-Peridinin-Protein-Complex (acpPC) from the coral symbiotic dinoflagellate *Symbiodinium*. *Photosynth. Res.* **2014**, *120*, 125–139. [[CrossRef](#)]
32. Jeffrey, S.t.; Humphrey, G. New spectrophotometric equations for determining chlorophylls a, b, c1 and c2 in higher plants, algae and natural phytoplankton. *Biochem. Physiol. Pflanz.* **1975**, *167*, 191–194. [[CrossRef](#)]
33. Veal, C.; Holmes, G.; Nunez, M.; Hoegh-Guldberg, O.; Osborn, J. A comparative study of methods for surface area and three-dimensional shape measurement of coral skeletons. *Limnol. Oceanogr. Methods* **2010**, *8*, 241–253. [[CrossRef](#)]
34. Asner, G.P.; Knapp, D.E.; Boardman, J.; Green, R.O.; Kennedy-Bowdoin, T.; Eastwood, M.; Martin, R.E.; Anderson, C.; Field, C.B. Carnegie Airborne Observatory-2: Increasing science data dimensionality via high-fidelity multi-sensor fusion. *Remote Sens. Environ.* **2012**, *124*, 454–465. [[CrossRef](#)]
35. Gao, B.C.; Goetz, A.F. Column atmospheric water vapor and vegetation liquid water retrievals from airborne imaging spectrometer data. *J. Geophys. Res. Atmos.* **1990**, *95*, 3549–3564. [[CrossRef](#)]
36. Thompson, D.R.; Gao, B.-C.; Green, R.O.; Roberts, D.A.; Dennison, P.E.; Lundeen, S.R. Atmospheric correction for global mapping spectroscopy: ATREM advances for the HypSPiRI preparatory campaign. *Remote Sens. Environ.* **2015**, *167*, 64–77. [[CrossRef](#)]
37. Feilhauer, H.; Asner, G.P.; Martin, R.E.; Schmidlein, S. Brightness-normalized partial least squares regression for hyperspectral data. *J. Quant. Spectrosc. Radiat. Transf.* **2010**, *111*, 1947–1957. [[CrossRef](#)]
38. Martens, H. Reliable and relevant modelling of real world data: A personal account of the development of PLS Regression. *Chemom. Intell. Lab. Syst.* **2001**, *58*, 85–95. [[CrossRef](#)]
39. Chen, S.; Hong, X.; Harris, C.J.; Sharkey, P.M. Sparse modeling using orthogonal forest regression with PRESS statistic and regularization. *IEEE Trans. Syst. Man. Cybern.* **2004**, *34*, 898–911. [[CrossRef](#)]
40. Harrison, D.E.; Asner, G.P. Sensitivity of spectral communities to shifts in benthic composition in Hawaiʻi. *Remote Sens. Environ.* **2024**. [[CrossRef](#)]
41. Tulloch, V.J.; Klein, C.J.; Jupiter, S.D.; Tulloch, A.I.; Roelfsema, C.; Possingham, H.P. Trade-offs between data resolution, accuracy, and cost when choosing information to plan reserves for coral reef ecosystems. *J. Environ. Manag.* **2017**, *188*, 108–119. [[CrossRef](#)]
42. Mumby, P.; Green, E.; Edwards, A.; Clark, C. Coral reef habitat mapping: How much detail can remote sensing provide? *Mar. Biol.* **1997**, *130*, 193–202. [[CrossRef](#)]
43. Asner, G.P.; Martin, R.E.; Knapp, D.E.; Tupayachi, R.; Anderson, C.; Carranza, L.; Martinez, P.; Houcheime, M.; Sinca, F.; Weiss, P. Spectroscopy of canopy chemicals in humid tropical forests. *Remote Sens. Environ.* **2011**, *115*, 3587–3598. [[CrossRef](#)]
44. Asner, G.P.; Martin, R.E.; Anderson, C.B.; Knapp, D.E. Quantifying forest canopy traits: Imaging spectroscopy versus field survey. *Remote Sens. Environ.* **2015**, *158*, 15–27. [[CrossRef](#)]
45. Lesser, M.; Mobley, C. Bathymetry, water optical properties, and benthic classification of coral reefs using hyperspectral remote sensing imagery. *Coral Reefs* **2007**, *26*, 819–829. [[CrossRef](#)]
46. Marco Agustín, L.-C.; Laura, F.-R.; Juan Sebastián, Z.-S.; Oscar, H.-R.; Carlos, L.-C. Correlation of chlorophyll a and total carotenoid concentrations with coral bleaching from locations on the Pacific coast of Mexico. *Mar. Freshw. Behav. Physiol.* **2006**, *39*, 279–291. [[CrossRef](#)]
47. Zhao, M.; Yu, K. Application of chlorophyll fluorescence technique in the study of coral symbiotic zooxanthellae micro-ecology. *Acta Ecol. Sin.* **2014**, *34*, 165–169. [[CrossRef](#)]
48. Wangpraseurt, D.; Larkum, A.W.; Ralph, P.J.; Kuhl, M. Light gradients and optical microniches in coral tissues. *Front. Microbiol.* **2012**, *3*, 316. [[CrossRef](#)] [[PubMed](#)]

49. Cunning, R.; Ritson-Williams, R.; Gates, R.D. Patterns of bleaching and recovery of *Montipora capitata* in Kāne ‘ohe Bay, Hawai ‘i, USA. *Mar. Ecol. Prog. Ser.* **2016**, *551*, 131–139. [[CrossRef](#)]
50. Wall, C.B.; Ritson-Williams, R.; Popp, B.N.; Gates, R.D. Spatial variation in the biochemical and isotopic composition of corals during bleaching and recovery. *Limnol. Oceanogr.* **2019**, *64*, 2011–2028. [[CrossRef](#)] [[PubMed](#)]
51. Drury, C.; Bean, N.K.; Harris, C.I.; Hancock, J.R.; Huckeba, J.; Roach, T.N.; Quinn, R.A.; Gates, R.D. Intrapopulation adaptive variance supports thermal tolerance in a reef-building coral. *Commun. Biol.* **2022**, *5*, 486. [[CrossRef](#)] [[PubMed](#)]
52. Pegau, W.S.; Gray, D.; Zaneveld, J.R.V. Absorption and attenuation of visible and near-infrared light in water: Dependence on temperature and salinity. *Appl. Opt.* **1997**, *36*, 6035–6046. [[CrossRef](#)] [[PubMed](#)]
53. Zeng, K.; Xu, Z.; Yang, Y.; Liu, Y.; Zhao, H.; Zhang, Y.; Xie, B.; Zhou, W.; Li, C.; Cao, W. In situ hyperspectral characteristics and the discriminative ability of remote sensing to coral species in the South China Sea. *GIScience Remote Sens.* **2022**, *59*, 272–294. [[CrossRef](#)]
54. Kok, J.; Bainbridge, S.; Olsen, M.; Rigby, P. Towards effective aerial drone-based hyperspectral remote sensing of coral reefs. In Proceedings of the Global Oceans 2020: Singapore–US Gulf Coast, Biloxi, MS, USA, 5–30 October 2020; pp. 1–6.

Disclaimer/Publisher’s Note: The statements, opinions and data contained in all publications are solely those of the individual author(s) and contributor(s) and not of MDPI and/or the editor(s). MDPI and/or the editor(s) disclaim responsibility for any injury to people or property resulting from any ideas, methods, instructions or products referred to in the content.